International Journal of Thermofluids 22 (2024) 100663

Contents lists available at ScienceDirect

International Journal of Thermofluids

journal homepage: www.sciencedirect.com/journal/international-journal-of-thermofluids

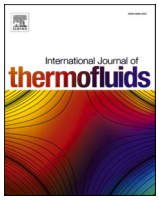

Development and investigation of a porous metal-ceramic substrate for solid oxide fuel cells

Serikzhan Opakhai [a,*], Kairat Kuterbekov [a], Zhasulan Zeinulla [a], Farruh Atamurotov [b,c,d]

[a] L.N. Gumilyov Eurasian National University, Faculty of Physics and Technical Sciences, Astana 010000, Kazakhstan
[b] New Uzbekistan University, Movarounnahr street 1, Tashkent 100000, Uzbekistan
[c] Institute of Theoretical Physics, National University of Uzbekistan, Tashkent 100174, Uzbekistan
[d] University of Tashkent for Applied Sciences, Str. Gavhar 1, Tashkent 100149, Uzbekistan

ARTICLE INFO

Keywords:
Thermal explosion
Metal-ceramic substrate
Porosity
Fuel cells
Exothermic reaction
Synthesis
Coefficient of thermal expansion

ABSTRACT

The process of creating a porous metal-ceramic material based on Ni-Al alloy and gadolinium-doped cerium oxide (CGO) using the thermal explosion method has been investigated. This study aims to analyze the effect of CGO on the thermal explosion parameters and the architecture of the resulting Ni-Al-CGO materials. In this regard, the influence of adding CGO powder to the Ni-Al system on the synthesis process and structure formation during controlled heat loss thermal explosion has been studied. Dependencies of temperature and time characteristics of the thermal explosion on initial parameters have been measured. It has been demonstrated that the concentration of CGO in the initial mixture and heat dissipation from the sample significantly affect the rate of the exothermic reaction. The phase composition of the obtained porous materials, depending on the CGO content and the temperature of subsequent vacuum annealing, was analyzed using X-ray diffraction. The chemical composition and microstructure of the synthesis products were examined through electron microscopy and energy-dispersive X-ray spectroscopy. The possibility of forming metal-ceramic composites with a porosity of 60–65 % for use as supporting substrates for solid oxide fuel cells with a NiO/CGO anode has been shown. An anodic layer of NiO/CGO was applied to a metal-ceramic base of the composition (Ni+25 %Al)+5 %CGO using screen printing, which was then annealed in an air atmosphere at 1300 °C and reduced at 900 °C in a hydrogen atmosphere. The dilatometric method determined that adding 40 wt.% Cr to a mixture of Ni-Al powders reduces the average coefficient of thermal expansion of the new material.

1. Introduction

Environmental pollutants due to the combustion of fossil fuels in conventional thermal power plants necessitate employment of alternative technologies and systems with low carbon emission for electricity generation. An interest in the novel and alternative sources of energy is sharply growing in the world [1]. Fuel cells are among the alternative clean energy technologies for power production with variety of applications, such as hybrid vehicles [1], unmanned aerial vehicle [2,3] and power generation in remote areas [4], with several advantages including high efficiency and possibility of operation independent from fossil fuels [5]. Fuel cell is an electrochemical technology, similar to battery, which produce electricity by exploitation of a chemical reaction. In contrast to battery, the required chemical for power generation are externally provided. In the majority of the cases, hydrogen and oxygen are the reactants of fuel cells [6]. Aside from stand-alone systems, it is possible to integrate fuel cells with other technologies for power generation [7]. There are different types of fuel cells with their own characteristics and operating principles such as proton exchange membrane fuel cell [8,9], solid oxide fuel cell (SOFC) [10], phosphoric acid fuel cell [11] etc. SOFC is one of the main types of fuel cells. These types of fuel cells have some advantages such as flexibility. Most fossil fuels, in both liquid and gaseous states, can in principle be applied as SOFC fuel for producing electricity. Despite the great potential of SOFC for meeting the challenges of future demand of energy, development of these types of fuel cells into commercial product is challenging [12]. These types of fuel cells have considerable potential to be integrated with different systems and technologies [13,14] or being used as stand-alone system for power generation.

An SOFC has three main components namely a porous cathode, a

* Corresponding author.
E-mail address: serikjan_0707@mail.ru (S. Opakhai).

https://doi.org/10.1016/j.ijft.2024.100663

Available online 13 April 2024

porous anode, and a dense electrolyte [15]. This kind of fuel cell is a solid-state converter of energy which is applied for direct conversion of fuels chemical energy into electricity via electrochemical reactions. SOFCs have not been developed for large-scale applications till now and their main constraints are lifetime and cost. The new design of the metal support has leads to possibility of improvement of an individual cell mechanical resistance, increment of battery thermal shock resistance and decrement in the SOFC system cost. As a consequence, metal-supported solid oxide fuel cells (MS-SOFCs) have received attention [16]. In comparison with the conventional ceramic-supported architectures, MS-SOFCs have some advantages like quick start-up, low cost, manufacturability and simplicity of sealing [17,18]. One of the promising areas for the use of porous metals is their use in MS-SOFCs [19]. Metal support structures have attracted much attention due to the possibility of rapid start-up, increased reliability, and resistance to thermal cycling compared to traditional SOFC, which use ceramic electrodes or electrolyte as a support base [20]. In addition, the transition to a design where a porous metal plate serves as a supporting base, and the electrolyte and electrodes are presented in the form of thin films, can reduce the cost of fuel cells [21].

The SOFC design on a supporting metal base is considered the most promising from the point of view of the possibility of reducing the thickness of the functional layers of the fuel cell, and as a result, reducing operating temperatures, increasing its reliability and durability. The supporting metal base is capable of providing the fuel cell with greater mechanical strength compared to cells on a supporting electrode or electrolyte, and therefore this design is attractive for use in mobile autonomous power plants. The presence of a rigid support allows the remaining electrochemically active layers of the fuel cell (electrodes and electrolyte) to be formed in the form of thin films. In this case, their thickness can be reduced to such a value that it is sufficient only to ensure the electrochemical function of the layer. But in practice, the thickness of the functional elements of a fuel cell is determined by the method of their formation. In a SOFC design with a supporting metal base, the formation of layers of an electrochemically active cell occurs on the surface of a porous and, as a rule, highly corrosion-resistant steel support [22,23].

For this, various powder technologies are used, such as slip casting, screen printing, sol-gel method and others that require high-temperature sintering. However, the use of these methods is associated with a number of difficulties. First of all, this concerns the oxidation of the metal base during the sintering of the anode layer, and as a result, a significant drop in its electrical conductivity and a decrease in the efficiency of SOFC in general. Therefore, a number of stringent requirements are imposed on materials intended for the manufacture of metal bases. First, such a material must have a coefficient of thermal expansion (CTE) close to the CTE of the remaining functional layers of the fuel cell to prevent mechanical destruction of the cell during thermal cycling from room to operating temperature of the SOFC. Secondly, the pore structure of the substrate material must ensure free access of reagents to the working zone and removal of reaction products from it, be resistant to a redox atmosphere, and also have chemical stability at SOFC operating temperatures [24,25].

The most commonly used metal substrate materials are Crofer 22 APU steel, as well as a small range of special iron-chromium steels produced by traditional metallurgical methods of sintering metal powders. A significant disadvantage of such materials is the presence of chromium in them, which, as a result of long-term operation of the fuel cell at SOFC operating temperatures (about 800 °C), is capable of diffusing to the anode surface with the formation of compounds such as Cr_2O_3, which destroy the anode and worsen its electrochemical characteristics [26,27]. To prevent this unwanted diffusion, barrier layers are formed on the surface of porous metal plates [28]. The purpose of such a barrier layer is to prevent mutual diffusion of the materials of the metal substrate and the anode layer. In addition, the barrier layer must be electrically conductive and not impede the gas flow, be close to the other layers of the CTE fuel cell, and also be mechanically and chemically resistant to the operating conditions of the SOFC. Spinels [29] or composites such as $La_{0.6}Sr_{0.2}Ca_{0.2}CrO_3$ [30], CeO_2 and $Ce_{0.8}Gd_{0.2}O_2$ [31] are used as effective diffusion barrier layers.

In most cases, stainless steels are commonly used to create supporting metallic substrates for SOFCs because they have a CTE close to the CTE of other components in the fuel cell and exhibit high oxidation resistance [31,32]. However, at high temperatures, a reaction occurs between iron (Fe) and chromium (Cr) from the metallic substrate, as well as nickel (Ni) from the anode, leading to a reduction in the catalytic activity of the latter [33]. To address this issue, diffusion barrier layers are applied between the metallic substrate and the anode [34,35]. Another approach to prevent the interaction of chromium with nickel involves using nickel-based metallic substrates [36], bimetallic compounds such as Ni-Fe [37,38], or Ni-Al [39].

To reduce the CTE of Ni-Al, the incorporation of a substance with a low CTE into the material is possible. In the study [40], various ceramic materials, such as ZrO_2, ZrO_2-SiO_2, Al_2TiO_5, Al_2O_3, and an unspecified oxide XO_2, were used as additives to Ni-Al [41]. It was experimentally established that adding an inert oxide XO_2 in the volume of 35–40 % reduces the CTE of the resulting composite to the level of 12×10^{-6} K^{-1} [42].

This study analyzed the impact of CGO on the parameters of thermal explosion and the structure of the resulting Ni-Al-CGO materials. CGO, with its high ionic conductivity ($9.50 \cdot 10^{-3}$ S/cm at 500 °C), is considered a potential electrolyte for SOFCs operating at temperatures below 700 °C [43]. In addition to high ionic conductivity, solid electrolytes based on CeO_2 are characterized by the absence of phase transitions in the temperature range from room temperature to the melting point. Their catalytic activity towards the direct oxidation of hydrocarbon fuel and chemical stability towards various electrode materials emphasize their promising application in SOFCs.

2. Methodology

The materials used in this study are presented in Table 1. Powder mixtures were prepared using a turbula mixer, and the composition of the mixture was selected according to the following ratio:

$$(1-x)\cdot([1-y]Ni + yAl) + xCGO \quad (1)$$

Compositions with mass concentrations of CGO in the range $x = 0$–30 % and mass concentration of aluminum in a mixture with nickel without taking into account the mass of CGO $y = 25$ % were studied. To simplify the recording of the composition, further in the text terms (1–x) and (1–y) will not be given, that is, the composition 75 %(75 %Ni+25 %Al)+ 25 %CGO will be written as (Ni+25 %Al)+25 %CGO.

The initial compressed sample was placed between two flat heat-removing stainless steel plates 5 mm thick. The pressing pressure of the plates to the sample PF = 0.18 MPa was set using a special press. The sample, clamped in the plates, was placed in an electric furnace in an argon environment (purity 99.999 %, pressure 0.10 MPa) and heated at a constant rate of 20 K/min. The sample temperature was controlled using a tungsten-rhenium thermocouple with a junction diameter of 0.1 mm, located near the sample surface. The thermocouple signal through the data acquisition system was recorded on a PC at a data acquisition rate of 250 Hz. After the synthesis, the resulting materials were cooled inside an electric furnace to room temperature in an argon environment (Fig. 1).

Table 1
Properties of the original reagent powders.

Powder	Particle size (μm)	Purity (%)	Source
Ni	3–7	99.8	Sigma-Aldrich
AI	60	99.9	Sigma-Aldrich
CGO	0.10–0.50	99.9	Sigma-Aldrich

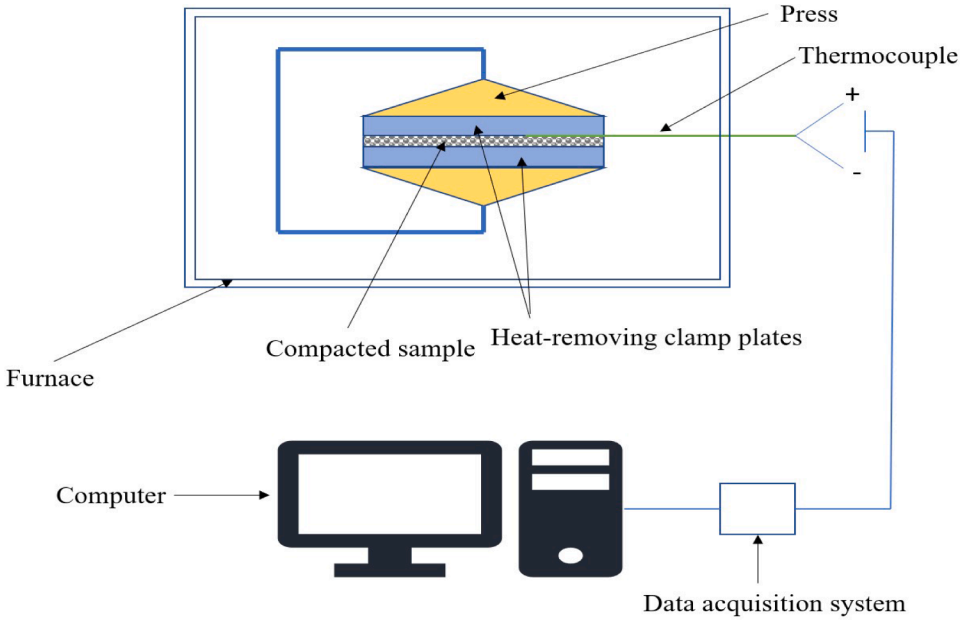

Fig. 1. Schematic diagram of thermal explosion reaction setup.

In order to determine the effect of annealing on the structure and composition of materials synthesized in the process of thermal explosion, they were heat treated in a vacuum furnace under conditions of heating and cooling at a rate of 10 K/min and holding at temperatures of 900–1200 °C for 2 h. In this case, the residual air pressure in the furnace was 10^{-2} Pa.

3. Results and discussion

3.1. Temperature dynamics of a thermal explosion

The standard stages of changing the temperature of a sample during a thermal explosion are presented in Fig. 2. In the first stage (stage 1), external heating of the sample at a constant rate is used to initiate a thermal explosion. At the second stage (stage 2), a rapid, almost linear increase in temperature occurs at a rate of 10^2–10^4 K/s, followed by a slowdown and reaching a maximum value. At this stage, an exothermic reaction of the mixture components actively occurs, in which the rate of heat release exceeds the rate of its transfer from the sample to the plates. After completion of the second stage, the cooling stage begins, characterized by a strong slowdown in the reaction, when heat transfer exceeds the rate of heat release in the sample.

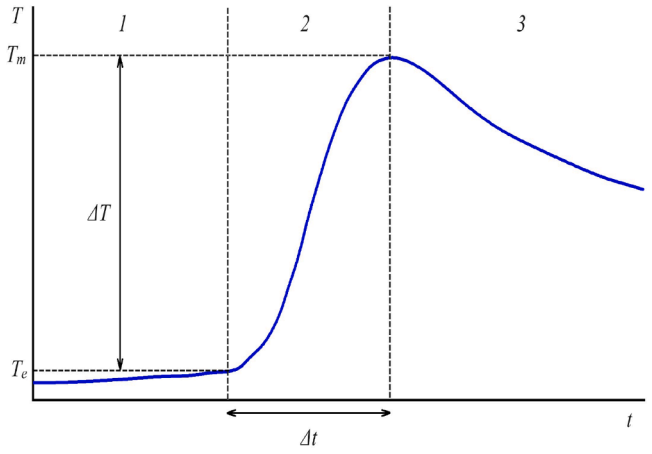

Fig. 2. Typical thermogram of the synthesis process in the mode of a mitigated thermal explosion.

By processing the thermogram data, the following thermal characteristics of the thermal explosion process were determined:

1. The temperature of the onset of a thermal explosion Te is the temperature at the conventional boundary of the intervals d2T/dt2 = 0 and d2T/dt2 >> 0.
2. Maximum process temperature T_m – temperature at point dT/dt = 0.
3. Thermal explosion amplitude $\Delta T = T_m - T_e$.
4. Duration of thermal explosion Δt – time of temperature change from T_e to T_m.

From the conducted experiments, it has been revealed that for samples with a thickness of 1 mm and a composition of Ni+25 %Al, a thermal explosion is observed only with the introduction of CGO up to 15 %. With the addition of 25 % CGO, no exothermic reaction is registered on the thermogram, and the sintering of the sample does not occur. In the case of samples with a thickness of 20 mm, synthesis is achieved for a composition with a higher content of the ceramic additive, namely (Ni+25 %Al)+25 %CGO. This is attributed to the minimal heat losses of the sample during the thermal explosion process, where the heat release rate exceeds the dynamics of heat dissipation.

The thermal explosion in thin samples occurs at a temperature around 600 °C. The amplitude of the thermal explosion decreases from 90 to 60 °C, and the duration of the explosion significantly increases with an increase in CGO concentration (Fig. 3, Table 2). In massive samples, a similar process exhibits a higher explosive preheating (up to 1300–1330 °C) and shorter duration (Fig. 4, Table 2). The onset temperature of the thermal explosion decreases to 570–510 °C, with the magnitude of the explosive preheating remaining almost unchanged upon the addition of CGO. This indicates the involvement of CGO in the exothermic chemical transformations of the system, as otherwise, a decrease in ΔT would be expected.

The most probable primary sources of heat release during the thermal explosion are the synthesis reactions of intermetallic alloys and the reduction of cerium oxide. These reactions occur concurrently in the Ni-Al and CeO_2 subsystems with aluminum according to the following gross schemes:

$$n_1Ni + n_2Al \rightarrow m_1NiAl + m_2Ni_3Al + H_1, \quad (2)$$

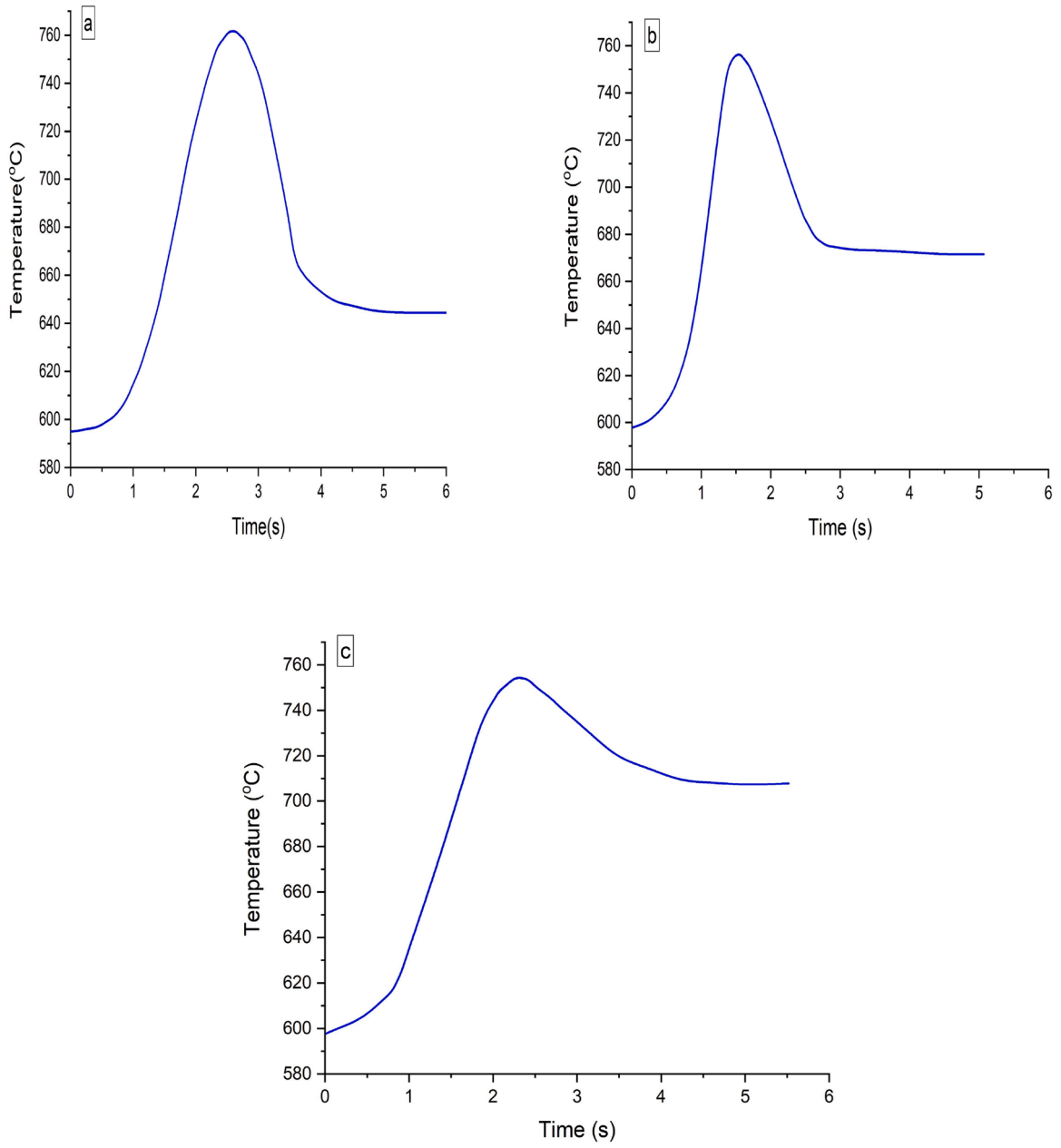

Fig. 3. Thermal explosion parameters of samples 1 mm thick: a – Ni+25 %Al, b – (Ni+25 %Al)+5 %CGO, c – (Ni+25 %Al)+15 %CGO.

Table 2
Parameters of thermal explosion of samples.

Sample size	Compound	Thermal explosion parameters		
		ΔT, °C	Δt, s	T_e, °C
Thickness 1mm	Ni+25 %Al	90	0.30	595
	(Ni+25 %Al)+5 %CGO	65	14.6	600
	(Ni+25 %Al)+15 %CGO	60	26.7	610
Thickness 20 mm	Ni+25 %Al	1330	2,8	570
	(Ni+25 %Al)+5%CGO	1320	3,2	560
	(Ni+25 %Al)+15 %CGO	1310	7,3	530
	(Ni+25 %Al)+25 %CGO	1305	8,2	510

$$c_1CeO_2 + c_2Al \rightarrow d_1CeAl_2 + d_2Al_2O_3 + H_2, \quad (3)$$

where n, m, c, d are the molar stoichiometric coefficients of the initial components and elements of the reaction, H_1, H_2 are the specific thermal effects of the reactions.

Thermal effects can be calculated using the formulas:

$$H_1 = \sum_i m_i \cdot \Delta H_i^{0'} - \sum_i n_i \cdot \Delta H_i^0, \quad (4)$$

$$H_2 = \sum_i c_i \cdot \Delta H_i^{0'} - \sum_i d_i \cdot \Delta H_i^0 \quad (5)$$

Here are the standard molar enthalpies of formation of the initial components and reaction products.

Taking into account the material balance of elements in reactions (2) and (3) and the possible variation in the ratio of the initial components in the Ni-Al and CeO_2-Al subsystems, calculation using formulas (4–5) shows that $H_1 \leq 0.9$ kJ/g, and $H_2 \leq 0.7$ kJ/g. It follows that the thermal effects of both reactions are comparable. It can be assumed that during a thermal explosion, the products of reactions (2) and (3) undergo further chemical transformations of the type and others.

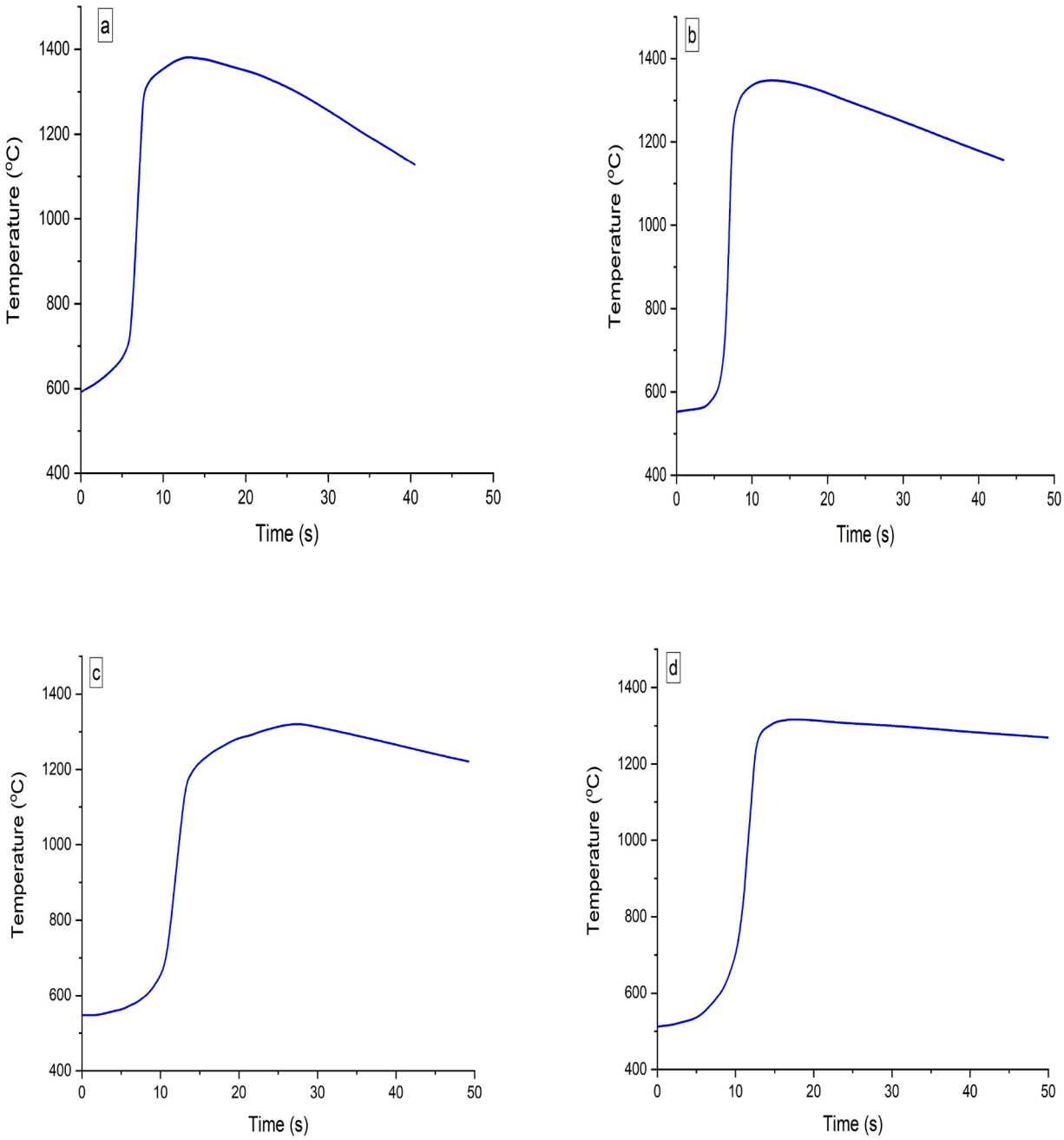

Fig. 4. Thermal explosion parameters of samples 20 mm thick: a – Ni+25 %Al, b – (Ni+25 %Al)+5 %CGO, c – (Ni+25 %Al)+15 %CGO, d – (Ni +25 %Al)+25 %CGO.

3.2. Phase composition and microstructure of synthesized materials

The phase composition of the synthesis products was analyzed depending on the content of CGO in the initial mixture and the temperature of subsequent annealing in a vacuum. The analysis results are presented in Table 3, Figs. 5 and 6.

According to the results of X-ray phase analysis, the synthesized compositions with CGO addition consist of a composite of phases:

Table 3
Phase composition of synthesized materials.

№	Compound	Annealing	Ni	Ni_2Al_3	NiAl	Ni_3Al	CGO	$CeAlO_3$
1	Ni+25 %Al	No	30	25	27	25	–	–
2	(Ni+25 %Al) + 5 % CGO	No	35	40	12	15	5	–
3	(Ni+25 %Al) + 15 % CGO	No	45	36	15	16	7	–
4	(Ni+25 %Al) + 25 % CGO	No	55	33	14	14	16	–
5	Ni+25 %Al	No	–	–	70	30	–	–
6	(Ni+25 %Al) + 15 % CGO	No	38	–	30	35	8	5
7	(Ni+25 %Al) + 15 % CGO	No	–	60	32	–	–	13

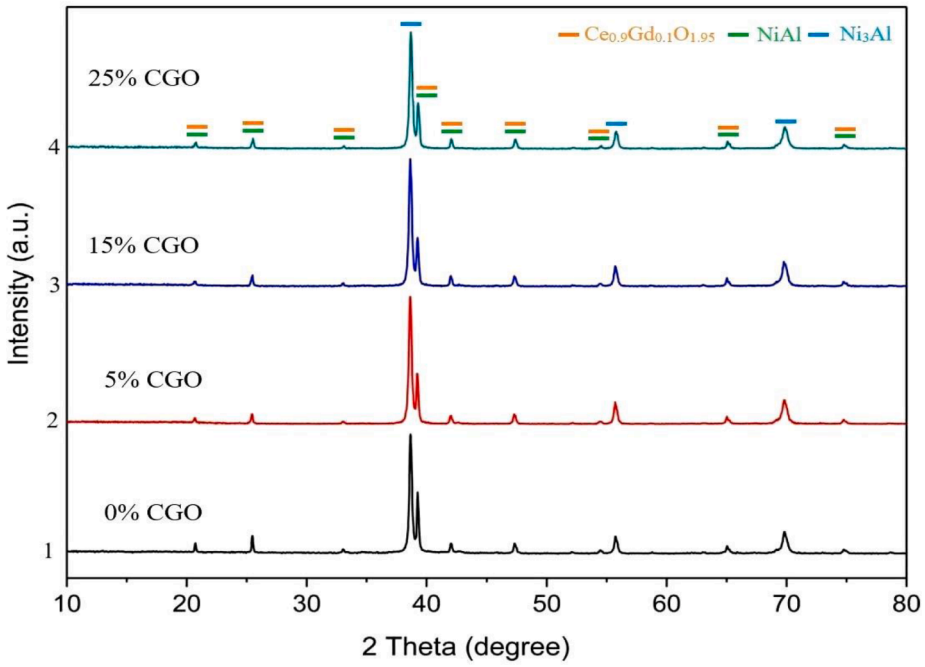

Fig. 5. Phase composition of 1 mm thick samples synthesized in the thermal explosion mode: 1 – composition Ni+25 %Al, 2 – composition (Ni+25 %Al) + 5 % CGO, 3 – composition (Ni+25 %Al) + 15 % CGO, 4 – composition (Ni+25 %Al) + 25 % CGO.

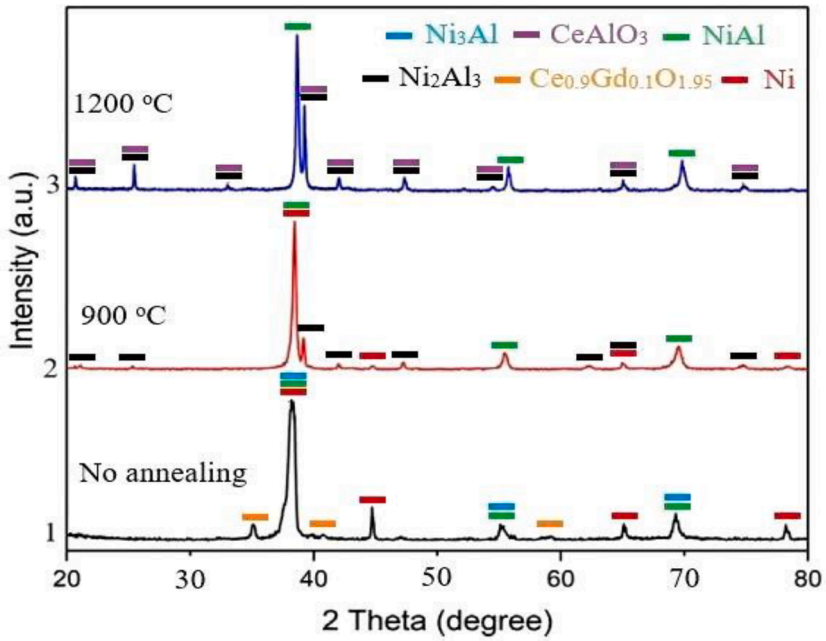

Fig. 6. Phase composition of samples (Ni+25 %Al) + 15 % CGO 1 mm thick: 1 – after synthesis in thermal explosion mode, 2 – after synthesis and annealing at a temperature of 900 °C, 3 – after synthesis and annealing at a temperature 1200 °C.

Ni_2Al_3, NiAl, Ni_3Al, Ni, and CGO. In this case, the synthesized material is also a porous skeleton consisting of welded composite particles. With the addition of 5 % CGO, the particles in the synthesis products also have a core structure with three layers: the inner layer is Ni, the intermediate layer is Ni_3Al, and the outer layer is NiAl. Moreover, according to X-ray microanalysis data, both outer layers contain traces of cerium. For the composition with 15 % CGO, such a layered structure is not observed along the entire perimeter of the nickel cores. This may indicate insufficient wettability of nickel particles surrounded by tiny CGO particles by the aluminum melt that is formed during the heating process. This is also confirmed by the detected slowdown of exothermic reactions during the thermal explosion (Fig. 5).

Annealing materials with CGO addition at 900 °C does not allow achieving the equilibrium composition of synthesis products due to the presence of a significant amount of unreacted nickel, in addition to intermetallic and oxide phases (sample №6, Table 3).

Vacuum annealing at a temperature of 1200 °C allowed obtaining a material with an equilibrium composition, including intermetallic phases NiAl and Ni_2Al_3 (sample №7, Table 3). An interesting observation is the detection of the perovskite-type phase $CeAlO_3$. According to

literature data, the formation of the perovskite-type phase $CeAlO_3$ during sintering of cerium oxide and aluminum powder typically occurs at temperatures significantly higher than 1200 °C [33]. Most likely, this phase is formed due to the oxidation of intermetallics Ce_xAl_y, which are formed during reaction (3). This conclusion is supported by the fact that when the synthesized samples were extracted from the reactor or samples after vacuum annealing, cooled to room temperature, they were observed to heat significantly upon contact with the atmospheric air. This heating is likely associated with the rapid oxidation of intermetallic phases formed during the synthesis and heat treatment of materials, such as the $CeAl_2$ phase (Fig. 6).

It was found that the composition of the synthesized materials differs significantly from the composition corresponding to the equilibrium state, as determined by the phase diagram of the Ni-Al system [31]. This occurs due to incomplete chemical conversion of the starting reagents during the thermal explosion process. Carrying out vacuum annealing of the synthesized material at a temperature of 900 °C for one hour makes it possible to bring its composition closer to equilibrium (sample №5, Table 3). Increasing the holding time does not affect the concentration of the constituent phases for samples without the addition of CGO.

The structure of the synthesis products of the Ni+25 %Al system is depicted in Fig. 7. The obtained material exhibits a porous structure formed by fused composite particles. Based on the phase diagram of the Ni-Al system, the chemical composition of the outer layer may consist of intermetallics such as Ni_2Al_3, NiAl, or their mixtures. The composition of the middle layer includes NiAl, Ni_3Al, or their combinations, while the core consists of a nickel-based solid solution. The sizes of the microcomposite particles in the synthesized products correspond to the nickel particles in the initial mixture. It can be assumed that during the thermal explosion, microcomposites form due to the capillary distribution of molten aluminum on the surface of nickel particles, followed by the reaction diffusion of components. The presence of round pores in the synthesized material indicates the action of capillary distribution corresponding to the original aluminum particles in both shape and size.

3.3. Formation of a NiO/CGO anode on the surface of a porous metal-ceramic base

On the metal bases of SOFCs, anode and electrolyte layers are formed, as a rule, using powder methods (screen printing, dipping or centrifugation, etc.), the final stage of which is high-temperature sintering of the applied layers [25]. In this case, sintering is carried out either in a reducing atmosphere (Ar/4 %H_2) [44], so as not to oxidize the metal base (Fe/Cr), or in an air atmosphere with subsequent reduction of the nickel-containing anode in a hydrogen atmosphere [35]. The latter approach has been used, for example, in the case of Ni-Fe alloy metal substrates.

In this work, we chose the same approach for sintering the anode layer, since the high Ni content in the starting material guarantees the preservation of the conductivity of the base after oxidation and subsequent reduction. An anodic layer of NiO/CGO was applied to a metal-ceramic base of the composition (Ni+25 %Al)+5 %CGO using screen printing, which was then annealed in an air atmosphere at 1300 °C and reduced at 900 °C in a hydrogen atmosphere. Fig. 8 shows the

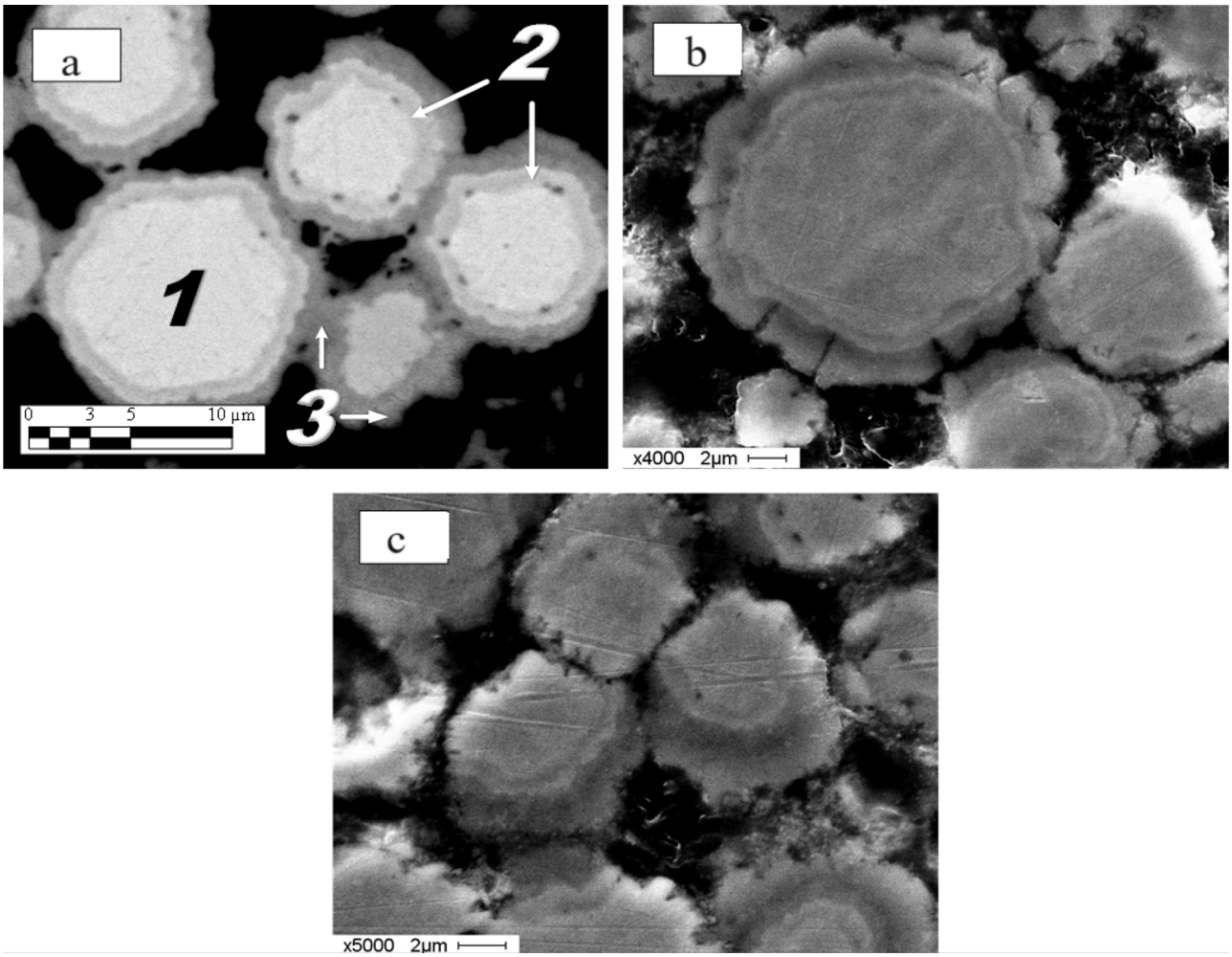

Fig. 7. Images of the synthesized composition product structures: a - Ni+25 %Al, b - (Ni+25 %Al)+5 %CGO, c - (Ni+25 %Al)+15 %CGO.

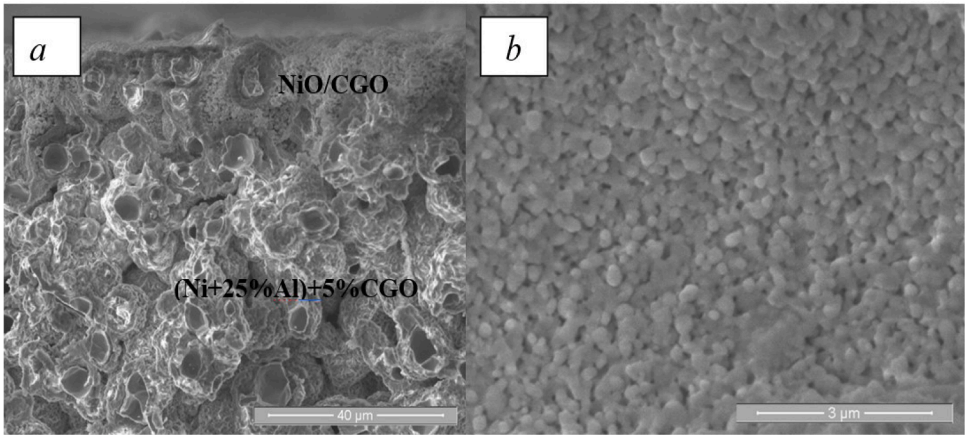

Fig. 8. Images of a chip of a (Ni+25 %Al)+5 %CGO base with a NiO/CGO anode (a) and the surface of a NiO/CGO anode sintered at 1300 °C in air and reduced at 900 °C in a hydrogen atmosphere (b).

microstructure of a metal-ceramic base with a NiO/CGO anodic layer about 20 μm thick sintered on its surface. After application, the anodic paste penetrates the surface of the porous material, which ensures good contact and adhesion to the base material after sintering. The anodic layer after sintering and reduction is a fairly smooth surface with a uniform nanoporous structure (pore size several hundred nanometers), on which a layer of CGO electrolyte can then be formed. X-ray phase analysis showed that after firing in an air atmosphere and reduction in hydrogen, the following changes occur in the phase composition of the metal-ceramic base: the content of the NiAl, Ni_3Al phases decreases and a thermodynamically stable α-Al_2O_3 phase appears. Since the content of conductive phases in the material remains high, the conductivity of the metal-ceramic base practically does not decrease.

3.4. Dilatometric measurements of the coefficient of thermal expansion of Ni-Ai and CGO composition

Fig. 9 shows the results of dilatometric studies of Ni-Al substrates in the temperature range from 30 to 1100 °C. The image shows that the temperature dependence of elongation dL/L for Ni-Al alloy is almost linear. The average coefficient of thermal expansion (CTE), determined on the basis of dilatometric measurements, is 14 × 10^{-6} K^{-1} over the temperature range from 700 to 900 °C. The measured value exceeds the CTE of SOFC layers (10–12 × 10^{-6} K^{-1}). However, research has shown that adding ceramic powder or refractory metal powder with a low coefficient of thermal expansion to the raw material mixture of Ni and Al powders can reduce the average CTE of the new material. For example, with the addition of 40 wt.% Cr (the CTE of pure Cr is 6.2 × 10^{-6} K^{-1}), the temperature dependence of the relative elongation dL/L of the Ni-Al+Cr sample agrees well with the same dependence for the Crofer 22 APU alloy samples. The CTE of Crofer 22 APU alloy is known to be 11 × 10^{-6} K^{-1}, and this material is widely used for the manufacture of SOFC carrier base [45]. Reducing the CTE of Ni-Al wafers by adding ceramic oxide powder has also been used in other studies [46]. The CTE was shown to be about 12 × 10^{-6} K^{-1} when using 30 % and 40 % ceramic oxide powder. One of the main advantages of large volume ceramic oxide powder is that the oxide powder physically dilutes the nickel aluminide combustion synthesis reaction, which prevents the development of a high-speed reaction front while maintaining dimensional stability of the part.

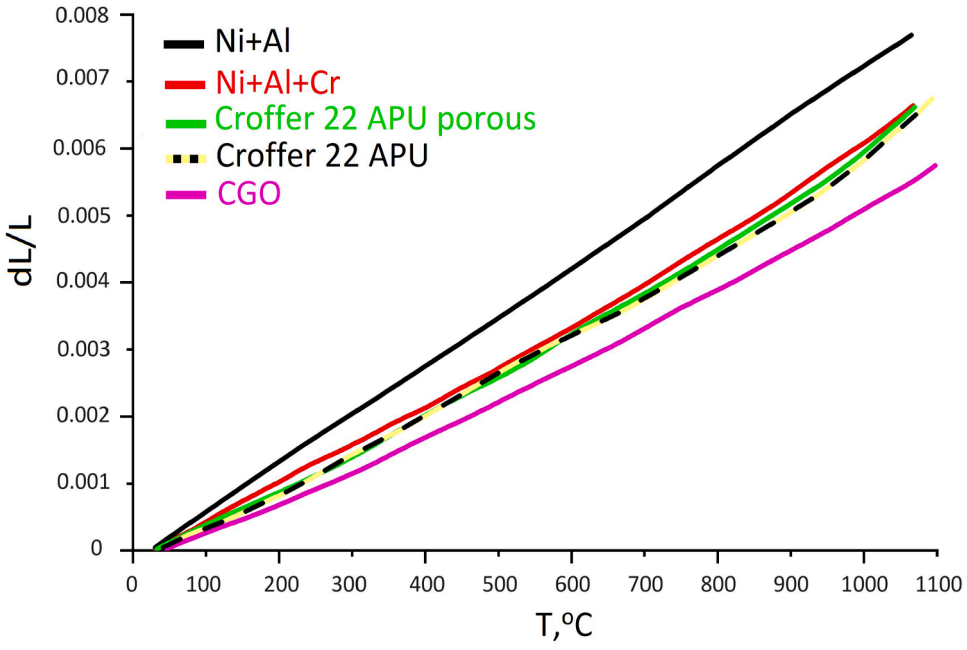

Fig. 9. Dependence of relative elongation on temperature for various SOFC materials.

4. Conclusion

In this work, we investigated the formation of a new metal-ceramic composite based on intermetallic compounds of the Ni-Al system and ceramics made of gadolinium-doped cerium oxide for use as a supporting base for medium-temperature solid oxide fuel cells with a NiO/CGO anode and a CGO electrolyte. The formation of porous metal-ceramics was carried out using the thermal explosion method. It has been shown that when synthesizing samples 1 mm thick under conditions of good heat removal (using heat-removing plates), adding up to 15 % CGO powder to the Ni+25 %Al system significantly reduces the intensity of the exothermic reaction. At a CGO concentration of more than 15 %, no exothermic reaction was observed.

When synthesizing samples 20 mm thick under conditions of poor heat removal from the reaction zone, the maximum process temperature Tm increased significantly (up to 1330 °C) and was practically independent of the CGO concentration. The synthesis product of the Ni + 25 %Al system was a porous material of sintered granules with a three-layer structure consisting of a core (nickel-based solid solution) surrounded by two layers of intermetallic compounds with different aluminum contents. When CGO was added to the initial mixture, the three-layer structure of the granule was maintained, and the CGO particles were dissolved in the middle and outer layers of the sintered granules.

X-ray phase analysis showed that the synthesized compositions with the addition of CGO consist of a composition of phases: Ni_2Al_3, NiAl, Ni_3Al, Ni and CGO. To bring the composition to an equilibrium state, the samples were vacuum annealed at a temperature of 1300 °C. The resulting material of the composition (Ni+25 %Al)+5 %CGO was used to form a two-layer structure of a metal-ceramic base - NiO/CGO anode of a solid oxide fuel cell. The latter was formed by screen printing followed by sintering in an air atmosphere and reduction in a hydrogen atmosphere. Vacuum annealing at a temperature of 1200 °C made it possible to obtain a material with an equilibrium composition, including intermetallic phases NiAl and Ni_2Al_3. Of interest is the discovery of the perovskite-type phase $CeAlO_3$. Carrying out vacuum annealing of the synthesized material at a temperature of 900 °C for one hour makes it possible to bring its composition closer to equilibrium. Increasing the holding time does not affect the concentration of the constituent phases for samples without the addition of CGO. The presence of oxide ceramics CGO and Al_2O_3 in the metal-ceramic base will lead to a decrease in the coefficient of thermal expansion of the Ni-Al system and its better correspondence to the CTE of SOFC layers (10–12 $\times$ 10^{-6} K^{-1}). The dilatometric method determined that adding 40 wt.% Cr to a mixture of Ni-Al powders reduces the average coefficient of thermal expansion of the new material.

CRediT authorship contribution statement

Serikzhan Opakhai: Writing – original draft, Supervision, Investigation, Funding acquisition, Formal analysis, Data curation, Conceptualization. **Kairat Kuterbekov:** Writing – review & editing, Methodology, Investigation. **Zhasulan Zeinulla:** Writing – review & editing, Methodology, Investigation. **Farruh Atamurotov:** Writing – review & editing, Investigation.

Declaration of competing interest

All the authors declare that they have no known competing financial interests or personal relationships that could have appeared to influence the work reported in this paper.

Data availability

Data will be made available on request.

Acknowledgments

The article was prepared as part of the implementation of the scientific project of grant funding for young scientists «Zhas Galym» for 2022–2024 of the Science Committee of the Ministry of Science and Higher Education of the Republic of Kazakhstan AP13268769 «Development and synthesis of a porous metal-ceramic base for thin-film SOFC».

References

[1] T. Taner, The novel and innovative design with using H2 fuel of PEM fuel cell: efficiency of thermodynamic analyze, Fuel 302 (2021) 121109, https://doi.org/10.1016/J.FUEL.2021.121109.
[2] M. Rostami, A.H. Farajollahi, F. Bagherpor, V. Sfandiyar, Reinforcing proton exchange membrane fuel cell powered unmanned aerial vehicle with an innovative combined flow field, Renew. Energy Res. Applic. 4 (2023) 87–101, https://doi.org/10.22044/RERA.2021.11214.1081.
[3] M. Rostami, A.H. Farajollahi, M. Marefati, R. Fili, F. Bagherpor, A comparative analysis and optimization of two supersonic hybrid solid oxide fuel cell and turbine-less jet engine propulsion systems for unmanned aerial vehicles, Renew. Energy Res. Applic. 3 (2022) 237–253, https://doi.org/10.22044/rera.2021.11173.1076.
[4] M.K. Singla, J. Gupta, P. Nijhawan, A.S. Oberoi, M.H. Alsharif, A. Jahid, Role of a unitized regenerative fuel cell in remote area power supply: a review, Energies 16 (2023) 5761, https://doi.org/10.3390/EN16155761, 2023, Vol. 16, Page 5761.
[5] M. Ramezanizadeh, M. Alhuyi Nazari, M. Hossein Ahmadi, L. Chen, A review on the approaches applied for cooling fuel cells, Int. J. Heat Mass Transf. 139 (2019) 517–525, https://doi.org/10.1016/J.IJHEATMASSTRANSFER.2019.05.032.
[6] P. Breeze, An introduction to fuel cells, Fuel Cell. (2017) 1–10, https://doi.org/10.1016/B978-0-08-101039-6.00001-7.
[7] R. Alayi, R. Seyednouri, M. Jahangiri, A. Ma'arif, Optimization, sensitivity analysis, and techno-economic evaluation of a multi-source system for an urban community: a case study, Renew. Energy Res. Applic. 3 (2022) 21–30, https://doi.org/10.22044/RERA.2021.10752.1054.
[8] T. Taner, Energy and exergy analyze of PEM fuel cell: a case study of modeling and simulations, Energy 143 (2018) 284–294, https://doi.org/10.1016/J.ENERGY.2017.10.102.
[9] T. Taner, The micro-scale modeling by experimental study in PEM fuel cell, J. Therm. Eng. 3 (2017) 1515–1526, https://doi.org/10.18186/JOURNAL-OF-THERMAL-ENGINEERING.331755.
[10] A. Kasaeian, M. Javidmehr, M.R. Mirzaie, L. Fereidooni, Integration of solid oxide fuel cells with solar energy systems: a review, Appl. Therm. Eng. 224 (2023) 120117, https://doi.org/10.1016/J.APPLTHERMALENG.2023.120117.
[11] S. Oh, T. Kim, S. Kim, S. Kang, Energetic, exergetic, economic, and exergoeconomic analysis of a phosphoric acid fuel cell-organic rankine cycle hybrid system, Energy Convers. Manag. 284 (2023) 116993, https://doi.org/10.1016/J.ENCONMAN.2023.116993.
[12] K. Huang, Solid oxide fuel cells, Mater. Fuel Cell. (2008) 280–343, https://doi.org/10.1533/9781845694838.280.
[13] A. Saberi Mehr, M. Ilkhani, S. Sabernia, S. Nooshmand, A. Ebrahimpour, B. Heydari, Thermodynamic modelling and optimisation of a green hydrogen-blended syngas-fueled integrated PV-SOFC system, Appl. Therm. Eng. 236 (2024) 121506, https://doi.org/10.1016/J.APPLTHERMALENG.2023.121506.
[14] Z. Lu, H. Zhang, L. Duan, Z. Wang, Q. Wang, A. Baccioli, U. Desideri, Exergoeconomic evaluation of novel solid oxide fuel cell-integrated solar combined cycle with different solar integration modes, Int. J. Hydrogen Energy 48 (2023) 18064–18082, https://doi.org/10.1016/J.IJHYDENE.2023.01.252.
[15] N.Q. Minh, Solid oxide fuel cell technology - features and applications, Solid State Ion. 174 (2004) 271–277, https://doi.org/10.1016/j.ssi.2004.07.042.
[16] S. Opakhai, K. Kuterbekov, Metal-supported solid oxide fuel cells: a review of recent developments and problems, Energies 16 (2023) 4700, https://doi.org/10.3390/EN16124700.
[17] K.J. Kim, B.H. Park, S.J. Kim, Y. Lee, H. Bae, G.M. Choi, Micro solid oxide fuel cell fabricated on porous stainless steel: a new strategy for enhanced thermal cycling ability, Sci. Rep. 6 (2016) 1–8, https://doi.org/10.1038/srep22443.
[18] T. Franco, M. Haydn, R. Mücke, A. Weber, M. Rüttinger, O. Büchler, S. Uhlenbruck, N.H. Menzler, A. Venskutonis, L.S. Sigl, Development of metal-supported solid oxide fuel cells, ECS Trans 35 (2011) 343, https://doi.org/10.1149/1.3570009.
[19] L.P. Lefebvre, J. Banhart, D.C. Dunand, Porous metals and metallic foams: current status and recent developments, Adv. Eng. Mater. 10 (2008) 775–787, https://doi.org/10.1002/ADEM.200800241.
[20] E. Dogdibegovic, R. Wang, G.Y. Lau, A. Karimaghaloo, M.H. Lee, M.C. Tucker, Progress in durability of metal-supported solid oxide fuel cells with infiltrated electrodes, J. Power Sources 437 (2019) 226935.
[21] A.A. Solovyev, S.V. Rabotkin, K.A. Kuterbekov, T.A. Koketay, S.A. Nurkenov, S. Opakhai, A.V. Shipilova, I.V. Ionov, G.M. Eliseeva, Comparison of sputter-deposited single and multilayer electrolytes based on gadolinia-doped ceria and yttria-stabilized zirconia for solid oxide fuel cells, Int. J. Electrochem. Sci. 15 (2020) 231–240, https://doi.org/10.20964/2020.01.43.
[22] V.V. Krishnan, Recent developments in metal-supported solid oxide fuel cells, Wiley Interdiscipl. Rev.: Energy Environ. 6 (2017) e246, https://doi.org/10.1002/WENE.246.

[23] M. Haydn, K. Ortner, T. Franco, N.H. Menzler, A. Venskutonis, L.S. Sigl, Development of metal supported solid oxide fuel cells based on powder metallurgical manufacturing route, Powder Metall. 8 (2013) 382–387, https://doi.org/10.1179/1743290113Y.0000000075.
[24] Y.B. Matus, L.C. De Jonghe, C.P. Jacobson, S.J. Visco, Metal-supported solid oxide fuel cell membranes for rapid thermal cycling, Solid State Ion. 176 (2005) 443–449, https://doi.org/10.1016/J.SSI.2004.09.056.
[25] M.C. Tucker, Progress in metal-supported solid oxide fuel cells: a review, J. Power Source. 195 (2010) 4570–4582, https://doi.org/10.1016/J.JPOWSOUR.2010.02.035.
[26] C.S. Hwang, C.H. Tsai, T.J. Hwang, C.L. Chang, S.F. Yang, J.K. Lin, Novel metal substrates for high power metal-supported solid oxide fuel cells, Fuel Cell. 16 (2016) 244–251, https://doi.org/10.1002/FUCE.201500216.
[27] J.J. Choi, J.H. Lee, D.S. Park, B.D. Hahn, W.H. Yoon, H.T. Lin, Oxidation resistance coating of LSM and LSCF on SOFC metallic interconnects by the aerosol deposition process, J. Am. Ceram. Soc. 90 (2007) 1926–1929, https://doi.org/10.1111/J.1551-2916.2007.01641.X.
[28] D. Roehrens, U. Packbier, Q. Fang, L. Blum, D. Sebold, M. Bram, N. Menzler, Operation of thin-film electrolyte metal-supported solid oxide fuel cells in lightweight and stationary stacks: material and microstructural aspects, Mater. (Basel) 9 (2016) 762, https://doi.org/10.3390/MA9090762.
[29] Z. Yang, J.S. Hardy, M.S. Walker, G. Xia, S.P. Simner, J.W. Stevenson, Structure and conductivity of thermally grown scales on Ferritic Fe-Cr-Mn steel for SOFC interconnect applications, J. Electrochem. Soc. 151 (2004) A1825, https://doi.org/10.1149/1.1797031/XML.
[30] T. Franco, K. Schibinger, Z. Ilhan, G. Schiller, A. Venskutonis, Ceramic diffusion barrier layers for metal supported SOFCs, ECS Trans. 7 (2007) 771–780, https://doi.org/10.1149/1.2729165/XML.
[31] M. Brandner, M. Bram, J. Froitzheim, H.P. Buchkremer, D. Stöver, Electrically conductive diffusion barrier layers for metal-supported SOFC, Solid State Ion. 179 (2008) 1501–1504, https://doi.org/10.1016/J.SSI.2008.03.002.
[32] Y. Zhou, X. Xin, J. Li, X. Ye, C. Xia, S. Wang, Z. Zhan, Performance and degradation of metal-supported solid oxide fuel cells with impregnated electrodes, Int. J. Hydrogen Energy 39 (2014) 2279–2285, https://doi.org/10.1016/J.IJHYDENE.2013.11.086.
[33] A.M. Dayaghi, K.J. Kim, S. Kim, J. Park, S.J. Kim, B.H. Park, G.M. Choi, Stainless steel-supported solid oxide fuel cell with La0.2Sr0.8Ti0.9Ni0.1O3−δ/yttria-stabilized zirconia composite anode, J. Power Source. 324 (2016) 288–293, https://doi.org/10.1016/J.JPOWSOUR.2016.05.076.
[34] J.J. Choi, J. Ryu, B.D. Hahn, C.W. Ahn, J.W. Kim, W.H. Yoon, D.S. Park, Low temperature preparation and characterization of solid oxide fuel cells on FeCr-based alloy support by aerosol deposition, Int. J. Hydrogen Energy 39 (2014) 12878–12883, https://doi.org/10.1016/J.IJHYDENE.2014.06.070.
[35] H.J. Cho, G.M. Choi, Fabrication and characterization of Ni-supported solid oxide fuel cell, Solid State Ion. 180 (2009) 792–795, https://doi.org/10.1016/J.SSI.2008.12.041.
[36] K.H. Kim, Y.M. Park, H. Kim, Fabrication and evaluation of the thin NiFe supported solid oxide fuel cell by co-firing method, Energy 35 (2010) 5385–5390, https://doi.org/10.1016/J.ENERGY.2010.07.018.
[37] H.J. Cho, K.J. Kim, Y.M. Park, G.M. Choi, Flexible solid oxide fuel cells supported on thin and porous metal, Int. J. Hydrogen Energy 41 (2016) 9577–9584, https://doi.org/10.1016/J.IJHYDENE.2016.04.040.
[38] V.A. Sadykov, V.V. Usoltsev, Y.E. Fedorova, V.A. Sobyanin, P.V. Kalinin, A. V. Arzhannikov, A.Y. Vlasov, M.V. Korobeinikov, A.A. Bryazgin, A.N. Salanov, M. R. Predtechenskii, O.F. Bobrenok, A.S. Ulikhin, N.F. Uvarov, O.L. Smorygo, A. F. Il'Yushchenko, V.Y. Ul'Yanitskii, S.B. Zlobin, Design of medium-temperature solid oxide fuel cells on porous supports of deformation strengthened Ni-Al alloy, Russ. J. Electrochem. 47 (2011) 488–493, https://doi.org/10.1134/S1023193511040148/METRICS.
[39] A.A. Solovyev, S.V. Rabotkin, A.V. Shipilova, A.I. Kirdyashkin, I.V. Ionov, A. N. Kovalchuk, A.S. Maznoy, V.D. Kitler, A.O. Borduleva, Solid oxide fuel cell with Ni–Al support, Int. J. Hydrogen Energy 40 (2015) 14077–14084, https://doi.org/10.1016/J.IJHYDENE.2015.07.151.
[40] Y. Fei, Thermal expansion, mineral physics and crystallography. A Handbook of Physical Constants, 1995.
[41] P. Timakul, S. Jinawath, P. Aungkavattana, Fabrication of electrolyte materials for solid oxide fuel cells by tape-casting, Ceram. Int. 34 (2008) 867–871, https://doi.org/10.1016/J.CERAMINT.2007.09.038.
[42] T.B. Massalski, H. Okamoto, P.R. Subramanian, L. Kacprzak. Binary Alloy Phase Diagrams, 2nd ed., ASM International, 1990.
[43] L. Vasylechko, A. Senyshyn, D. Trots, R. Niewa, W. Schnelle, M. Knapp, $CeAlO_3$ and $Ce_{1-x}R_xAlO_3$ (R=La, Nd) solid solutions: crystal structure, thermal expansion and phase transitions, J. Solid State Chem. 180 (2007) 1277–1290, https://doi.org/10.1016/J.JSSC.2007.01.020.
[44] D. Roehrens, F. Han, M. Haydn, W. Schafbauer, D. Sebold, N.H. Menzler, H. P. Buchkremer, Advances beyond traditional SOFC cell designs, Int. J. Hydrogen Energy 40 (2015) 11538–11542, https://doi.org/10.1016/J.IJHYDENE.2015.01.155.
[45] A. Topcu, B. Öztürk, Ö.N. Cora, Performance evaluation of machined and powder metallurgically fabricated Crofer®22 APU interconnects for SOFC applications, Int. J. Hydrogen Energy 47 (2022) 3437–3448, https://doi.org/10.1016/J.IJHYDENE.2021.06.036.
[46] A. Smirnova, V. Sadykov, N. Mezentseva, V. Usoltsev, O. Smorygo, O. Bobrenok, N. Uvarov, Metal-supported SOFC on compressed Ni-Al foam substrates, in: ASME 2010 8th International Conference on Fuel Cell Science, Engineering and Technology, FUELCELL 2010 2, 2010, pp. 411–416, https://doi.org/10.1115/FUELCELL2010-33268.